

Theoretical Investigations on the Roles of Intramolecular Structure Distortion versus Irregular Intermolecular Packing in Optical Spectra of 6T Nanoparticles

Wenqiang Li,[†] Qian Peng,^{*,‡} Huili Ma,[†] Jin Wen,[§] Jing Ma,[§] Linda A. Peteanu,^{||} and Zhigang Shuai^{*,†}

[†]Key Laboratory of Organic OptoElectronics and Molecular Engineering, Department of Chemistry, Tsinghua University, Beijing 100084, P. R. China

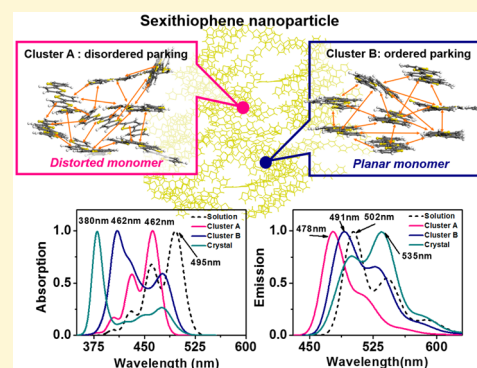
[‡]Key laboratory of Organic Solids, Institute of Chemistry, Beijing National Laboratory for Molecular Sciences, Chinese Academy of Sciences, Beijing 100190, P. R. China

[§]Institute of Theoretical and Computational Chemistry, Key Laboratory of Mesoscopic Chemistry of MOE, School of Chemistry and Chemical Engineering, Nanjing University, Nanjing 210093, P. R. China

^{||}Department of Chemistry, Carnegie Mellon University, 4400 Fifth Avenue, Pittsburgh, Pennsylvania 15213, United States

Supporting Information

ABSTRACT: It is of vital importance to theoretically understand unique nanoparticle size-tunable and excitation wavelength-dependent multiple optical properties in organic nanoparticles. In this work, we proposed a theoretical protocol to calculate the optical spectrum of the organic nanoparticles, which combines molecular dynamics (MD) simulation, the quantum mechanics/molecular mechanics (QM/MM) approach, and vibronic-coupled Frenkel exciton spectrum theory. By using the protocol, we explored the relationship between intramolecular structure distortion, irregular intermolecular packing, and optical spectra in α -sexithiophene nanoparticles. Two representative clusters cutting from the simulated amorphous nanoparticle were investigated and found to exhibit a blue shift for absorption and emission spectra compared to the solution, which is totally different from the blue-shifted absorption and red-shifted emission in crystal. For the cluster with distorted monomer and disordered packing, the blue shift results from the higher excitation energy and larger vibronic coupling of low-frequency vibration modes, while for the cluster with planar monomer and ordered packing, the blue shift is induced by the synergism of vibronic coupling and excitonic coupling. Strikingly, the superposition of the spectra of two clusters reproduces the experimental spectra and well explains the unusual blue-shifted emission observed for α -sexithiophene nanoparticles. Our theoretical protocol is general and applicable to other organic nanoparticles, thus aiding the rational design of high-quality organic nanoparticles.



1. INTRODUCTION

Organic nanoparticles have attracted significant research interests for their promising potential applications in nanoscale optoelectronic devices owing to their unique luminescent properties, such as nanoparticle size-tunable optical property,¹ multicolor emissions,² excitation wavelength-dependent multiple emissions,³ and so on.⁴ Recently, a newly prepared α -sexithiophene (α 6T) nanoparticle with a diameter range from 100 to 200 nm was found to exhibit a blue shift in both absorption and emission spectra compared to the solution,⁵ which is quite different from the previous reported red shift in emission upon aggregate in crystal,⁶ thin film,⁷ and nanoaggregates.^{8,9} Understanding the luminescent mechanism of the organic nanoparticle is of great importance for designing and achieving excellent organic opto-functional nanomaterials. Through experimental measurements, some explanations have

been inferred. For instance, the red shift in the absorption spectrum of 1-phenyl-3-((dimethylamino)-styryl)-5-((dimethylamino)phenyl)-2-pyrazoline (PDDP) nanoparticles relative to the solution was thought to be caused by the charge transfer (CT) exciton confinement effect.¹⁰ The hypochromic shift in the emission spectrum of 1,3-diphenyl-5-(2-anthryl)-2-pyrazoline (DAP) nanoparticle was ascribed to the restriction of the vibronic relaxation in aggregate.¹ The multiple emissions of 1,3-diphenyl-5-pyrenyl-2-pyrazoline (DPP) were claimed to be resulting from the formation of the CT complex and surface effect.³ The multicolor emissions of 1,2,3,4,5-pentaphenyl-1,3-

Special Issue: Computational Design of Functional Materials

Received: October 3, 2016

Revised: January 23, 2017

Published: January 23, 2017

cyclopentadiene (PPCP) nanoribbon with blue-green-red color were attributed to three different kinds of emitting centers coexisting in it, which correspond to the high-energy transition from single PPCP molecules and low-energy transition induced by the crystallinity and the structural defect.² However, the microstructure of the nanoparticle and the origin of its unusual optical properties are still unclear due to the limitations of the experimental conditions and techniques.

Theoretically, the optical spectra of organic compounds in crystalline and amorphous phases have been investigated in many groups. By using a Frenkel polaron model coupled with the experimental parameters, Spano et al. have explored the feature of 0–0 and 0–1 transition intensities in H- and J-type crystalline conformations by considering molecular energetic disorder, structural defects, and multiple mode exciton–phonon coupling.^{11–14} Applying the mixed Frenkel exciton and charge transfer exciton model, Liang et al. attributed the large red-shifted emission of 3,4,9,10-perylenetetracarboxylic diimide (PTCDI) to the intermolecular charge transfer character by considering an effective normal mode.¹⁵ Through molecular dynamics (MD) simulation and time-dependent density functional theory (TDDFT) calculations, Ma et al. claimed that the blue shift in absorption of $\alpha 6T$ nanoparticle results from the formation of the high-energy distorted chains.^{5,16} Using the multimode-coupled spectral theory of an isolated molecule and combined MD simulations and quantum mechanics/molecular mechanics (QM/MM) calculations, Shuai et al. explored the relationship among molecular packing, optical spectra, and fluorescence quantum efficiency of hexaphenylsilole nanoparticles and revealed that the decreased reorganization energy results in the blue shift of the emission spectra from amorphous to crystalline phases.¹⁷ Gierschner et al. treated the vibronic coupling in the molecular crystal based on pure quantum chemical cluster calculations.¹⁸

In this work, we proposed a calculation scheme combining MD simulation, the QM/MM approach, and the vibronic-coupled Frenkel exciton theory to comprehensively investigate the optical spectra of the organic nanoparticle, exemplified by a commonly used optoelectronic component $\alpha 6T$ (Figure 1).

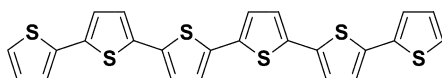


Figure 1. Chemical structure of $\alpha 6T$.

Our protocol successfully explored the relationship between the irregular molecular packing, the molecular structure distortion or planarity, and the optical property in $\alpha 6T$ nanoparticles from first-principles, which can provide a deep understanding of the luminescent mechanism of unique optical features in organic nanoparticles.

2. METHODOLOGY

2.1. Vibronic-Coupled Frenkel Exciton Model. The model Hamiltonians of the vibronic-coupled exciton are expressed as¹⁹

$$\hat{H} = \sum_{m,n} J_{mn} a_m^\dagger a_n + \sum_{n,k} \omega_n b_{nk}^\dagger b_{nk} + \sum_{n,k} \omega_{nk} g_{nk} a_m^\dagger a_n (b_{nk}^\dagger + b_{nk}) \quad (1)$$

Here, a_n^\dagger (a_n) is the creation (annihilation) operator for the excited state on molecule n and b_{nk}^\dagger (b_{nk}) is the creation (annihilation) operator for the k th vibrational mode on molecule n . J_{mn} represents the excitonic coupling between molecules m and n , ω_{nk} and g_{nk} are the frequency

and vibronic coupling strength of the k th vibrational mode on molecule n ($g_{nk}^2 = S_{nk}$ is the Huang–Rhys factor).

Under the Frenkel exciton model, which assumes only one molecule is electronically excited in the aggregate, the basis function of the aggregate (containing p monomers) can be expressed in the excited state as

$$|e, n\rangle = |g(1), \dots, g(n-1), e(n), g(n+1), \dots, g(p)\rangle \quad (2)$$

and in the ground state,

$$|g\rangle = |g(1), g(2), \dots, g(p)\rangle \quad (3)$$

in which

$$|g(n)\rangle = |\Phi_n^g\rangle \prod_k (b_k^\dagger)^{\nu_k} |0_k\rangle \quad (4)$$

$$|e(n)\rangle = |\Phi_n^e\rangle \prod_k (\tilde{b}_k^\dagger)^{\tilde{\nu}_k} |\tilde{0}_k\rangle \quad (5)$$

are the wave functions of the n th monomer in the electronic ground and excited states with k th vibrational mode with a quanta ν_k ($\tilde{\nu}_k$), respectively. Then, applying the Lang–Firsov canonical transformation,²⁰ the Hamiltonian can be transformed to

$$\hat{H} = \sum_{m,n} J_{mn} \tilde{a}_m^\dagger \tilde{a}_n + \sum_{n,k} \omega_n b_{nk}^\dagger b_{nk} \quad (6)$$

$$\tilde{a}_m^\dagger = e^{\sum_k -s_k (b_{mk} - b_{mk}^\dagger)} a_m^\dagger \quad (7)$$

Inserting eq 6 into the basis functions, the model Hamiltonian matrix of an aggregate in the excited state is obtained,^{21,22}

$$H = \begin{bmatrix} H_1 & J_{12} & \dots & J_{1,p-1} & J_{1,p} \\ J_{21} & H_2 & \dots & J_{2,p-1} & J_{2,p} \\ \dots & \dots & \dots & \dots & \dots \\ J_{p-1,1} & J_{p-1,2} & \dots & H_{p-1} & J_{p-1,p} \\ J_{p,1} & J_{p,2} & \dots & J_{p,p-1} & H_p \end{bmatrix} \quad (8)$$

with

$$H_n = \langle e, n | \hat{H} | e, n \rangle = \langle e(n) | \hat{H} | e(n) \rangle + \sum_{m \neq n}^p \langle g(m) | \hat{H} | g(m) \rangle \quad (9)$$

$$J_{m,n} = \langle g | \tilde{a}_m \hat{H} \tilde{a}_n^\dagger | g \rangle = \langle e, m | \hat{H} | e, n \rangle \quad (10)$$

The elements in the matrix in eq 8 can be further calculated according to refs 23 and 24. Then, based on the eigenvalue and eigenstate of the aggregate's excited state, obtained by diagonalizing the matrix eq 8, the absorption and emission spectra can be calculated by using the following equations:^{25–27}

$$\sigma_{\text{abs}}(\omega) = \frac{4\pi^2 \omega}{3\hbar c} |\vec{\mu}|^2 |FC|^2 \delta(\Delta\varepsilon - \omega) \quad (11)$$

$$\sigma_{\text{emi}}(\omega) = \frac{4\pi^2 \omega^3}{3\hbar c^3} |\vec{\mu}|^2 |FC|^2 \delta(\Delta\varepsilon - \omega) \quad (12)$$

Here, $\vec{\mu}$ is the electric transition dipole moment of monomer and $\Delta\varepsilon$ is the energy difference between the aggregate's excited state and its ground state. The FC is the Franck–Condon integral between the eigenstate of the aggregate's excited and ground states, in which the temperature effect is taken into account by Boltzmann distribution of the initial state.

2.2. Computational Details. The MD simulation was performed in the NVT system with the polymer consistent force field (PCFF).^{16,28} After equilibrium, one snapshot was extracted from the MD trajectories, as in our former work,⁵ to set up QM/MM models. We first sought two representative chains having effective conjugation lengths (ECL) of 3 and 6, respectively. Then, we took the chain (ECL

= 3 or 6) as the central QM part and the surrounding chains, which is less than 30 Å away from the central chain, as the MM part (the MM part is frozen, see Figure 2a). For the crystal, the QM/MM model was

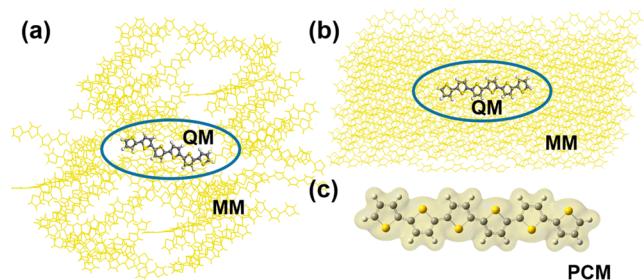


Figure 2. Construction of the QM/MM models for $\alpha 6T$ in nanoparticle (a) and crystal (b) state and PCM model (c).

constructed by cutting a cluster from the X-ray crystal structure of size $5 \times 5 \times 3$, and the central chain is treated using QM and the surrounding ones are treated by MM (see Figure 2b). The QM/MM calculations were accomplished using the ChemShell 3.5 program.²⁹ The QM calculations were performed at the B3LYP^{30,31}/6-31G(d) level in the Turbomole 6.5 program.^{32,33} The MM calculations were implemented by using the general Amber force field (GAFF)³⁴ in the DL-POLY program.³⁵ The selection of PCFF for MD simulation and GAFF for MM calculation is discussed in the Supporting Information. The restrained electrostatic potential was treated at the HF/6-31G(d) level. Finally, the adiabatic excitation energy was adjusted by the CAM-B3LYP³⁶ functional. The $\alpha 6T$ in tetrahydrofuran was evaluated by adopting the polarizable continuum model (PCM)³⁷ with $\epsilon = 7.43$ (see Figure 2c). Linear-response (LR) PCM³⁸ was applied to the geometric optimization and frequency calculations and state-specific (SS) PCM^{39,40} was used to calculate the excitation energy at the CAM-B3LYP/6-31G(d) level in the Gaussian 09 D01 program.⁴¹

The optical spectra were evaluated by employing the vibrationally coupled Frenkel exciton theory in the MOMAP program.⁴² The excitonic coupling was calculated using the tools in the MOMAP program based on the excitation information obtained from TDDFT calculations in the NWchem 6.3 program⁴³ at the CAM-B3LYP/6-31G(d) level. Seven normal vibrational modes were selected by their Huang–Rhys factors and vibrational frequency distribution feature (details in Supporting Information, Tables S1 and S2). The vibrational quantum number $\tilde{\nu}_k$ was determined by the Franck–Condon integral $f_{k, \tilde{\nu}_k=0}^i$, and the threshold was set to 1% of the maximum. The Gaussian half-width γ was set to 1100 cm^{-1} in all the spectra calculations at room temperature, since this value was shown to be suitable for oligothiophene systems in ref 44.

3. RESULTS AND DISCUSSION

3.1. Irregular Molecular Packing and Excitonic Interaction in $\alpha 6T$ Nanoparticles. To characterize the molecular packing in $\alpha 6T$ nanoparticles, MD simulations were performed in 0.1:1 THF/water solution at 298 K using the canonical (NVT) ensemble and polymer consistent force field (PCFF²⁸) in ref 5. The simulated results indicate that the geometrical structures of the constituent chains have different ECL values ranging from 2 (extremely distorted chain) to 6 (planar chain). Here, the monomers having an ECL of 3 and 6 were present in the highest percentages in the statistical distribution derived from MD simulations. Therefore, we selected two representative clusters, which were cut from the simulated nanoparticle having central monomers of ECL = 3 (cluster A) and ECL = 6 (cluster B), to investigate the optical properties of the nanoparticle. To confirm that clusters A and B were representative of the whole, we did the same statistics to characterize the intrachain torsion and interchain packing as

those done in ref 5, including torsion angle (α) and interchain distance (d), inclination angle (θ), and orientation angle (β). These are given in Figure S2 of the Supporting Information. It is found that the distributions of the values of α , d , θ , and β calculated for clusters A and B are very similar to those of the entire nanoparticle given in ref 5. Moreover, the interchain packings of these clusters exhibit typical π -stacked and T-shaped structures. This demonstrates that clusters A and B are suitable to be used to investigate the optical properties of the nanoparticle. In addition, the cluster cut from the X-ray crystal structure was studied for comparison.⁶

Considering the delocalization of Frenkel exciton, the clusters consisting of a central monomer and its surrounding molecules are used as the computational model (8 molecules for cluster A/B and 9 molecules for crystal, seen in Figure 3a,c,f) to calculate the excitonic couplings J . The excitonic

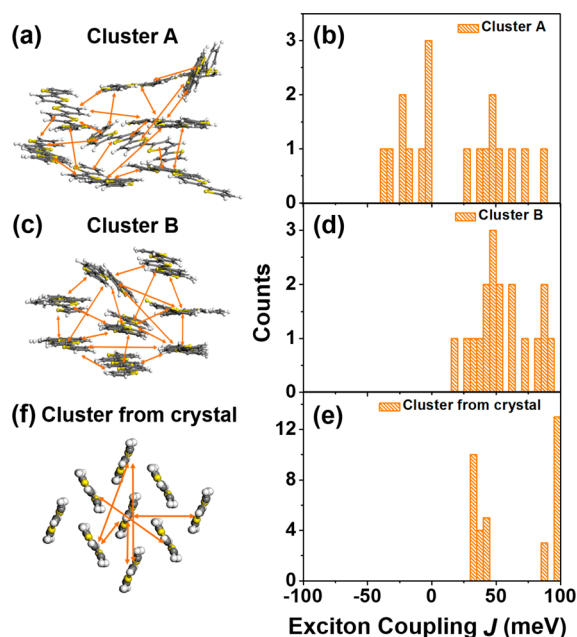


Figure 3. Packing structure and histogram of excitonic coupling J (arrows in the figure represent the pairs that are considered to have an effective excitonic coupling) of cluster A (a, b), cluster B (c, d), and crystal (e, f).

couplings between nearest-neighbor molecules and next-nearest-neighbor ones were calculated based on the TDDFT transition densities for the clusters, and the results are given in Figure 1b,d,e (detailed data can be found in Figures S3–S5, Supporting Information). It is easily seen from Figure 3 that the chain stacking in cluster A appears to be very disordered and the resultant excitonic couplings are diverse and range from negative to positive values (from -37.9 to 85.1 meV). This indicates the coexistence of head-to-tail J-aggregation and face-to-face H-aggregation. In contrast, the chain packing in cluster B is more ordered and compact relative to that in cluster A, and pure H-aggregation is seen with positive excitonic couplings varying from 15.3 to 92.3 meV . As expected, the crystal exhibits a perfectly symmetric herringbone structure with larger excitonic couplings of 30.2 – 96.4 meV . On the whole, the excitonic couplings in the three clusters are very large and would be expected to have a drastic influence on the optical spectra.

3.2. Multimode Vibronic Coupling Feature of Monomer. To examine the degree of structural disorder and the intramolecular vibronic coupling features in different phases, we first optimized the geometrical and electronic structures and calculated the vibrational frequencies. The combined QM/MM approach was used for the expanded clusters A and B with a radius of 30 Å and crystal cluster with a size of $5 \times 5 \times 3$, in which the central monomer acts as the QM part and the surrounding chains are treated as the MM part. As found in previous work, the dihedral angles between two adjacent thiophene rings are readily modified when the surrounding environment changes. Therefore, we focused on the five dihedral angles at the ground and the first excited singlet states as shown in Figure 4. The following are found: (i) The chain

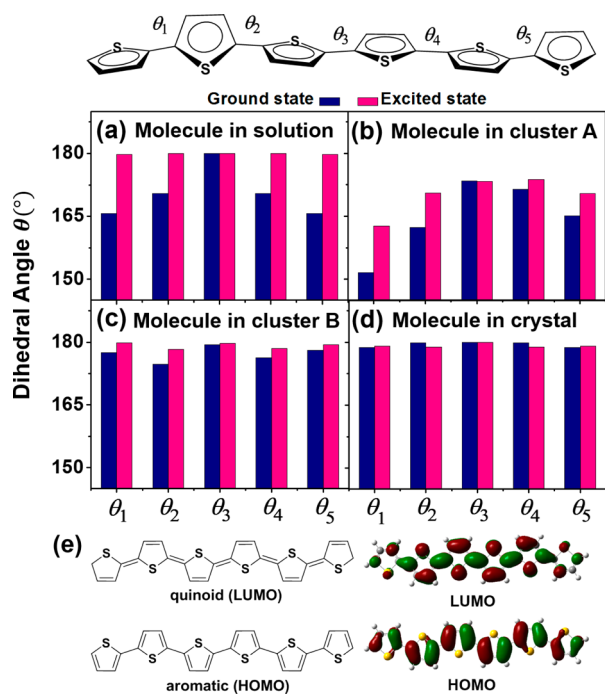


Figure 4. Selected dihedral angles of equilibrium geometry structures in solution (a), cluster A (b), cluster B (c), and crystal (d) at the ground and excited states; frontier molecular orbital future, aromatic, and quinoid structures of $a6T$ (e).

becomes more planar from the ground state to the first excited singlet states in all the cases because the geometrical structure transforms from aromatic to quinoidal character (see HOMO and LUMO orbitals in Figure 4e).^{45–47} (ii) The degree of chain distortion in the ground state is increased in the order crystal, cluster B, solution, and cluster A, which leads to an increase in the vertical energy in the same order. (iii) The most significant differences between the ground and the excited states are in solution and in cluster A. In both cases, free motion is possible due to weak intermolecular interactions. This also indicates that the vibronic coupling during the transition process would be relatively strong in these two cases. (iv) The terminal thiophene rings in a chain are more sensitive to the environment than are the central ones. For instance, the dihedral angle θ_3 is almost 180° in all cases, while θ_1 and θ_5 vary significantly among chains. (v) Chains that are completely free in solution or are in an extremely compact crystalline phase retain their symmetry well, while the chain symmetry is significantly lower in the nanoparticles due to the relatively disordered packing.

The Huang–Rhys factor (S) is a good parameter to characterize the degree of the vibronic couplings.⁴⁸ The S of the i th normal mode can be calculated by using $S_i = \omega_i \Delta D^2 / (2\hbar)$, where ω_i is the frequency and ΔD is the displacement of the i th normal mode. The calculated results at the ground and the first excited singlet states are plotted in Figure 5 and Figure

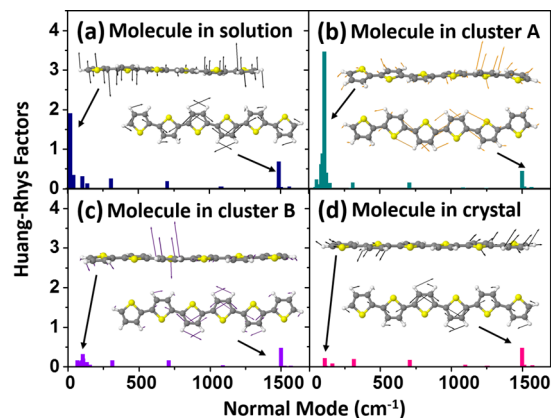


Figure 5. Calculated Huang–Rhys factors versus the displacement of the main normal modes in solution, cluster A, cluster B, and crystal.

S6 in the Supporting Information, respectively. As seen in Figure 5, the Huang–Rhys factors increase significantly moving from crystal/cluster B to solution/cluster A. The main contributions to S come from low-frequency normal modes ($<200 \text{ cm}^{-1}$), which are related to the distorted vibrational motion out of the backbone plane. Therefore, the more the geometry of the monomer is distorted, the larger the Huang–Rhys factor is. Moreover, twisting motion is sensitive to the surrounding environment. The high-frequency normal modes (around 1500 cm^{-1}), which are the C–C stretching vibrations in thiophene rings, are similar in all cases and insensitive to the molecular geometry and environment. Also seen in Figure 5, there are many normal modes whose contributions to Huang–Rhys factors are comparable and necessary to model the spectra, especially for the cluster A and the molecule in solution.

3.3. Vibrationally Resolved Optical Spectra of Nanoparticle and Crystal. Based on the geometrical and electronic structures obtained from QM/MM calculations, the vibrationally resolved optical spectra of the investigated clusters were calculated by using the vibronic-coupled Frenkel exciton model and plotted in Figure 6. In the calculations, the involved normal modes and vibrational quantum number are given in Table S1 of Supporting Information. In order to clearly measure the effect of the excitonic coupling, we calculated the optical spectrum of the monomer (QM molecule) in the QM/MM model. This was set as a reference and also plotted in Figure 6. For cluster A, both the absorption and the emission spectra of monomer and cluster are completely overlapped, which indicates that the excitonic interactions do not have any impact on the spectra. For cluster B, relative to the absorption and emission of the monomer, the absorption of cluster exhibits a large blue shift while the emission of cluster shows a slight red shift and a decrease in intensity. This is because the 0–0 peak is suppressed and the higher Frenkel exciton state therefore becomes dominant, which is the typical behavior of H-aggregation. For the crystal, this trend is even more notable due to its strong H-aggregation packing. In addition, only

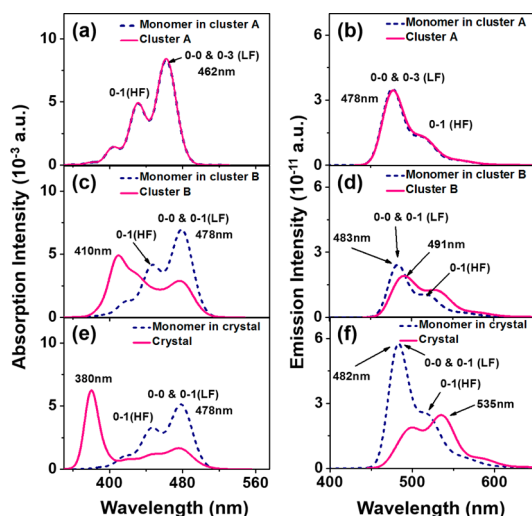


Figure 6. Calculated absorption and emission spectra of cluster A (a, b), cluster B (c, d), and crystal (e, f) at 298 K. LF denotes low-frequency normal modes and HF represents high-frequency normal modes.

considering the effect of structural distortion, the absorption of a distorted monomer in cluster A is blue-shifted by 16 nm and the emission is blue-shifted by 5 nm relative to those of planar monomer in cluster B.

Also seen in Figure 6, the optical spectra of the three clusters exhibit fine structures owing to strong intramolecular vibronic coupling. In order to obtain insight into the role of the intramolecular vibronic coupling on the optical spectrum, we further compared the optical spectra by accounting for different normal modes. According to the vibronic coupling model discussed above, we divided the normal modes into two categories: low-frequency ($<200\text{ cm}^{-1}$) normal modes and high-frequency (ca. 1500 cm^{-1}) ones. These two kinds of normal modes were considered in the calculated emission spectra in Figure 7. It is clear that, when only considering the

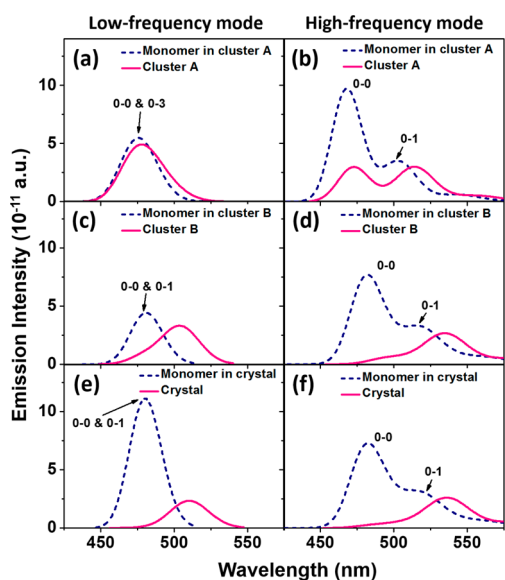


Figure 7. Calculated emission spectra induced by the vibronic coupling of low-frequency normal mode (a, c, and e) and high-frequency normal mode (b, d, and f) of cluster A at 298 K.

low-frequency modes, the spectra appear as a single peak. This is because the $0-n$ ($n \geq 1$) peak is extremely close to the $0-0$ peak owing to very small energy gap. However, as a matter of fact, the dominance between $0-0$ and $0-n$ peaks is determined by the vibronic coupling of the low-frequency modes. For instance, the largest Huang–Rhys factor of the low-frequency mode is 3.46, and therefore the $0-3$ peak is dominant in cluster A. In contrast, because the largest Huang–Rhys factors are 0.32 and 0.21 in cluster B and crystal, respectively, the $0-0$ peak overwhelms the $0-1$ peak for both. Based on the Frenkel exciton model, the $0-0$ peak is suppressed in H-aggregation but is red-shifted and strengthened in intensity in J-aggregation. Likewise, the $0-n$ peak is red-shifted in H-aggregation and red-shifted and weakened in intensity in J-aggregation.^{11,23,49}

Therefore, as seen in Figure 7c,e, the emission of cluster B and crystal manifest a large red shift compared to the monomer due to their pure H-aggregation. In contrast, the emission of cluster A exhibits a slight shift due to the disordered stacking of mixed H- and J-aggregations.

When only high-frequency normal modes are considered, the monomer emission exhibits two main peaks arising from the $0-0$ and $0-1$ transitions because $S < 1$ in three cases (see Figure 7b,d,f). As the excitonic coupling is included, the $0-0$ peak disappears and the $0-1$ peak is red-shifted, resulting in only a single peak in the emission spectra of the cluster B and in the crystal (Figure 5d,f). The emission of cluster A still displays two peaks owing to its disordered structure. This analysis reveals that the multimode vibronic couplings are of vital importance to correctly modeling the optical spectrum in addition to the excitonic interaction.

The effect of disordered aggregation on the optical spectra can be more clearly seen in Figure 8. The trimer extracted from

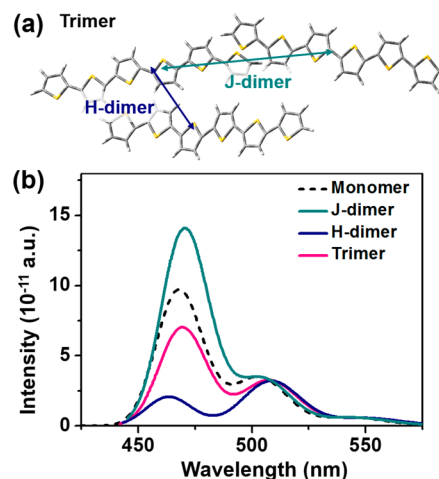


Figure 8. Calculated emission spectra of monomer, dimer, and trimer extracted from cluster A at 298 K.

cluster A includes H-dimer and J-dimer interactions. Compared to the emission of the monomer, the maximum peak of emission of the H-dimer is strongly red-shifted (Figure 8) due to the suppression of the $0-0$ peak and the red shift of the $0-1$ peak while the emission of the J-dimer is slightly red-shifted because of the enhanced $0-0$ peak and the diminished $0-1$ peak. The emission of the trimer is the superimposition of H-dimer and J-dimer emissions to some extent.

3.4. Interpretation of Blue-Shifted Absorption and Emission of α 6T Nanoparticles. In experiments, a variety of

absorption and emission bands were observed in α 6T nanoparticles.⁵ Distinct from the more commonly observed red-shifted emission upon aggregation, a surprising blue shift of the emission was found for the first time in α 6T nanoparticles. The mechanism underlying the variety in emission wavelengths observed for α 6T was not known prior to this study. Strikingly, our calculations successfully identified the origin of the excitation wavelength-dependent absorption and multicolor luminescence. We compare the calculated optical spectra in solution and in different clusters with the experimental counterparts in Figure 9. First, relative to the solution-phase

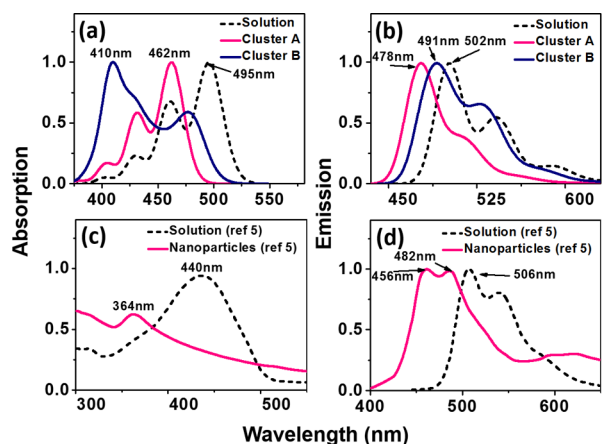


Figure 9. Comparison between the calculated absorption (a) and emission (b) and the experiment counterparts (c and d) at 298 K. Reprinted with permission from ref 5. Copyright 2014 American Chemical Society.

absorption, the blue shift value of the maximum peak is calculated to be 33 nm (0.18 eV) for cluster A and 85 nm (0.52 eV) for cluster B. The latter is closer to the experimental 76 nm (0.59 eV) in ref 5. Therefore, the observed large blue shift in absorption is attributed to the formation of an H-aggregate-like cluster B. Second, the calculated emission spectra better reproduce the experiment both in solution and in nanoparticles. The two main peaks observed experimentally can be identified with cluster A and B, respectively. Collectively, disordered molecular structure and intermolecular packing induce the unusual optical spectra phenomena observed in α 6T nanoparticles. It should be noted here that the H-aggregate can emit significant light via the other vibronic progressions although the 0–0 transition is forbidden.⁴⁹ The obtained radiative decay rate constant by integrating over the whole emission spectrum of cluster B in Figure 6d is decreased by ca. 5% relative to that of monomer. In contrast, the radiative rate constant of cluster A obtained from Figure 6b is almost unchanged after considering exciton coupling.

4. CONCLUSION

We proposed a theoretical scheme to calculate the optical spectrum of nanoparticles which combines molecular dynamics (MD) simulations, quantum mechanics/molecular mechanics (QM/MM) calculations, and vibronically coupled Frenkel exciton spectrum calculations. Using this scheme, we explored the relationship between irregular molecular packing, diverse molecular structural distortions, and optical spectra in α -sexithiophene nanoparticles. From the structures derived from MD simulations, we chose two representative clusters with

central monomer of ECL = 3 (cluster A) and ECL = 6 (cluster B) from the simulated amorphous nanoparticle for investigation, as well as one cluster cut from the X-ray crystal structure for comparison. For cluster A, the monomer is significantly distorted and the intermolecular packing is largely disordered. These factors give rise to a higher excitation energy and multimode vibronic coupling that result in a blue shift of the optical spectra. Excitonic interaction can be neglected owing to the mutually canceling effect of H- and J-type coupling in these distorted structures. For cluster B, the monomer is almost planar and the intermolecular packing is H-aggregate-like and relatively ordered. Consequently, the synergism of the multimode vibronic coupling and the excitonic interaction results in a sharp blue shift of the optical spectra. The optical spectra of both cluster A and cluster B are totally different from the blue shift of absorption and red shift of emission predicted for a crystal with strong H-aggregation. Notably, the superimposition of the spectra of these two cluster types reproduces the experimental results and explains the unique spectral properties of the α -sexithiophene nanoparticles. Our theoretical protocol successfully elucidates the relationship among the irregular molecular packing, diverse molecular structure distortion, and optical spectra in organic nanoparticles. This protocol is general and applicable to the study of the optical properties of other organic nanoparticles.

■ ASSOCIATED CONTENT

Supporting Information

The Supporting Information is available free of charge on the ACS Publications website at DOI: 10.1021/acs.chemmater.6b04210.

Comparisons of PCFF and GAFF force field. Statistical analysis of the α 6T clusters A and B and nanoparticle from ref 5. Packing structure and excitonic coupling in cluster A, cluster B, and crystal from crystal. Calculated Huang–Rhys factors in excited state. Selected ground/excited state normal modes and their quantum number in this calculation (PDF)

■ AUTHOR INFORMATION

Corresponding Authors

*E-mail: qpeng@iccas.ac.cn (Q.P.).

*E-mail: zgshuai@tsinghua.edu.cn (Z.S.).

ORCID

Jing Ma: 0000-0001-5848-9775

Linda A. Peteanu: 0000-0003-0075-6521

Zhigang Shuai: 0000-0003-3867-2331

Notes

The authors declare no competing financial interest.

■ ACKNOWLEDGMENTS

Illuminating discussions with Prof. Wanzhen Liang (Xiamen University) and Dr. Yingli Niu are greatly acknowledged. Q.P. and Z.S. thank the National Natural Science Foundation of China (Grants 21473214, 21290191, 21503118, and 91233105), the Ministry of Science and Technology of China through the 973 program (Grants 2013CB834703, 2015CB65502, and 2013CB933503), and the Strategic Priority Research Program of the Chinese Academy of Sciences (Grant XDB12020200). L.A.P. acknowledges NSF CHE-1012529 for financial support.

REFERENCES

- (1) Xiao, D.; Xi, L.; Yang, W.; Fu, H.; Shuai, Z.; Fang, Y.; Yao, J. Size-tunable emission from 1,3-diphenyl-5-(2-anthryl)-2-pyrazoline nanoparticles. *J. Am. Chem. Soc.* **2003**, *125*, 6740–6745.
- (2) Zhao, Y. S.; Fu, H.; Hu, F.; Peng, A. D.; Yao, J. Multicolor emission from ordered assemblies of organic 1d nanomaterials. *Adv. Mater.* **2007**, *19*, 3554–3558.
- (3) Fu, H.; Loo, B. H.; Xiao, D.; Xie, R.; Ji, X.; Yao, J.; Zhang, B.; Zhang, L. Multiple emissions from 1,3-diphenyl-5-pyrenyl-2-pyrazoline nanoparticles: evolution from molecular to nanoscale to bulk materials. *Angew. Chem., Int. Ed.* **2002**, *41*, 962–965.
- (4) Zhao, Y. S.; Fu, H.; Peng, A.; Ma, Y.; Xiao, D.; Yao, J. Low-dimensional nanomaterials based on small organic molecules: preparation and optoelectronic properties. *Adv. Mater.* **2008**, *20*, 2859–2876.
- (5) Hong, J.; Jeon, S.; Kim, J. J.; Devi, D.; Chacon-Madrid, K.; Lee, W.; Koo, S. M.; Wildeman, J.; Sfeir, M. Y.; Peteanu, L. A.; Wen, J.; Ma, J. The effects of side-chain-induced disorder on the emission spectra and quantum yields of oligothiophene nanoaggregates: a combined experimental and md-tddft study. *J. Phys. Chem. A* **2014**, *118*, 10464–10473.
- (6) Muccini, M. Low energy electronic and optical properties of α -sexithiophene single crystals. *Mater. Sci. Eng., C* **1998**, *5*, 173–177.
- (7) Yassar, A.; Horowitz, G.; Valat, P.; Wintgens, V.; Hmyene, M.; Deloffre, F.; Srivastava, P.; Lang, P.; Garnier, F. Exciton coupling effects in the absorption and photoluminescence of sexithiophene derivatives. *J. Phys. Chem.* **1995**, *99*, 9155–9159.
- (8) Nepomnyashchii, A. B.; Ono, R. J.; Lyons, D. M.; Sessler, J. L.; Bielawski, C. W.; Bard, A. J. Oligothiophene nanoparticles: photophysical and electrogenerated chemiluminescence studies. *J. Phys. Chem. Lett.* **2012**, *3*, 2035–2038.
- (9) Ostrowski, D. P.; Lytwak, L. A.; Mejia, M. L.; Stevenson, K. J.; Holliday, B. J.; Vanden Bout, D. A. The effects of aggregation on electronic and optical properties of oligothiophene particles. *ACS Nano* **2012**, *6*, 5507–5513.
- (10) Fu, H. B.; Yao, J. N. Size effects on the optical properties of organic nanoparticles. *J. Am. Chem. Soc.* **2001**, *123*, 1434–1439.
- (11) Spano, F. C. The spectral signatures of frenkel polarons in H- and J-aggregates. *Acc. Chem. Res.* **2010**, *43*, 429–439.
- (12) Spano, F. C. Excitons in conjugated oligomer aggregates, films, and crystals. *Annu. Rev. Phys. Chem.* **2006**, *57*, 217–243.
- (13) Zhao, Z.; Spano, F. C. Multiple mode exciton-phonon coupling: Applications to photoluminescence in oligothiophene thin films. *J. Phys. Chem. C* **2007**, *111*, 6113–6123.
- (14) Spano, F. C. Absorption and emission in oligo-phenylene vinylene nanoaggregates: The role of disorder and structural defects. *J. Chem. Phys.* **2002**, *116*, 5877–5891.
- (15) Gao, F.; Liang, W.; Zhao, Y. Theoretical studies of vibrationally resolved absorption and emission spectra: From a single chromophore to multichromophoric oligomers/aggregates. *Sci. China: Chem.* **2010**, *53*, 297–309.
- (16) Zhang, G.; Pei, Y.; Ma, J.; Yin, K.; Chen, C.-L. Packing structures and packing effects on excitation energies of amorphous phase oligothiophenes. *J. Phys. Chem. B* **2004**, *108*, 6988–6995.
- (17) Zheng, X.; Peng, Q.; Zhu, L.; Xie, Y.; Huang, X.; Shuai, Z. Unraveling the aggregation effect on amorphous phase AIE luminogens: a computational study. *Nanoscale* **2016**, *8*, 15173–15180.
- (18) Wykes, M.; Pambill, R.; Beljonne, D.; Gierschner, J. Vibronic coupling in molecular crystals: a franck-condon herzberg-teller model of h-aggregate fluorescence based on quantum chemical cluster calculations. *J. Chem. Phys.* **2015**, *143*, 114116.
- (19) May, V.; Kühn, O. *Charge and Energy Transfer Dynamics in Molecular Systems*; Wiley-VCH: Weinheim, 2004.
- (20) Hoffmann, M.; Soos, Z. G. Optical absorption spectra of the Holstein molecular crystal for weak and intermediate electronic coupling. *Phys. Rev. B: Condens. Matter Mater. Phys.* **2002**, *66*, 024305.
- (21) Gao, F.; Liang, W. Z.; Zhao, Y. Vibrationally resolved absorption and emission spectra of rubrene multichromophores: temperature and aggregation effects. *J. Phys. Chem. A* **2009**, *113*, 12847–12856.
- (22) Seibt, J.; Marquetand, P.; Engel, V.; Chen, Z.; Dehm, V.; Würthner, F. On the geometry dependence of molecular dimer spectra with an application to aggregates of perylene bisimide. *Chem. Phys.* **2006**, *328*, 354–362.
- (23) Li, W.; Peng, Q.; Xie, Y.; Zhang, T.; Shuai, Z. Effect of intermolecular excited-state interaction on vibrationally resolved optical spectra in organic molecular aggregates. *Huaxue Xuebao* **2016**, *74*, 902–909.
- (24) Hsu, C.-P.; You, Z.-Q.; Chen, H.-C. Characterization of the short-range couplings in excitation energy transfer. *J. Phys. Chem. C* **2008**, *112*, 1204–1212.
- (25) Valeur, B.; Berberan-Santos, M. N. *Molecular Fluorescence*; Wiley-VCH: Weinheim, 2012.
- (26) Lin, C.-K.; Li, M.-C.; Yamaki, M.; Hayashi, M.; Lin, S. H. A theoretical study on the spectroscopy and the radiative and non-radiative relaxation rate constants of the S01A1-S11A2 vibronic transitions of formaldehyde. *Phys. Chem. Chem. Phys.* **2010**, *12*, 11432–11444.
- (27) Shuai, Z.; Peng, Q. Organic light-emitting diodes: theoretical understanding of highly efficient materials and development of computational methodology. *Nat. Sci. Rev.* **2016**, nww024.
- (28) Sun, H. Ab initio calculations and force field development for computer simulation of polysilanes. *Macromolecules* **1995**, *28*, 701–712.
- (29) Sherwood, P.; de Vries, A. H.; Guest, M. F.; Schreckenbach, G.; Catlow, C. R. A.; French, S. A.; Sokol, A. A.; Bromley, S. T.; Thiel, W.; Turner, A. J.; Billeter, S.; Terstegen, F.; Thiel, S.; Kendrick, J.; Rogers, S. C.; Casci, J.; Watson, M.; King, F.; Karlsen, E.; Sjøvoll, M.; Fahmi, A.; Schäfer, A.; Lennartz, C. QUASI: A general purpose implementation of the QM/MM approach and its application to problems in catalysis. *J. Mol. Struct.: THEOCHEM* **2003**, *632*, 1–28.
- (30) Becke, A. D. Density-functional thermochemistry. III. The role of exact exchange. *J. Chem. Phys.* **1993**, *98*, 5648–5652.
- (31) Lee, C.; Yang, W.; Parr, R. G. Development of the Colle-Salvetti correlation-energy formula into a functional of the electron density. *Phys. Rev. B: Condens. Matter Mater. Phys.* **1988**, *37*, 785–789.
- (32) TURBOMOLE, version 6.5; University of Karlsruhe and of the Forschungszentrum Karlsruhe GmbH: 2013 (TURBOLE GmbH, since 2007).
- (33) Ahlrichs, R.; Bär, M.; Häser, M.; Horn, H.; Kölmel, C. Electronic structure calculations on workstation computers: The program system turbomole. *Chem. Phys. Lett.* **1989**, *162*, 165–169.
- (34) Wang, J.; Wolf, R. M.; Caldwell, J. W.; Kollman, P. A.; Case, D. A. Development and testing of a general amber force field. *J. Comput. Chem.* **2004**, *25*, 1157–1174.
- (35) Smith, W.; Forester, T. R. DL_POLY_2.0: A general-purpose parallel molecular dynamics simulation package. *J. Mol. Graphics* **1996**, *14*, 136–141.
- (36) Yanai, T.; Tew, D. P.; Handy, N. C. A new hybrid exchange–correlation functional using the coulomb-attenuating method (CAM-B3LYP). *Chem. Phys. Lett.* **2004**, *393*, 51–57.
- (37) Tomasi, J.; Mennucci, B.; Cammi, R. Quantum mechanical continuum solvation models. *Chem. Rev.* **2005**, *105*, 2999–3093.
- (38) Scalmani, G.; Frisch, M. J.; Mennucci, B.; Tomasi, J.; Cammi, R.; Barone, V. Geometries and properties of excited states in the gas phase and in solution: theory and application of a time-dependent density functional theory polarizable continuum model. *J. Chem. Phys.* **2006**, *124*, 094107.
- (39) Impropa, R.; Barone, V.; Scalmani, G.; Frisch, M. J. A state-specific polarizable continuum model time dependent density functional theory method for excited state calculations in solution. *J. Chem. Phys.* **2006**, *125*, 054103.
- (40) Impropa, R.; Scalmani, G.; Frisch, M. J.; Barone, V. Toward effective and reliable fluorescence energies in solution by a new state specific polarizable continuum model time dependent density functional theory approach. *J. Chem. Phys.* **2007**, *127*, 074504.
- (41) Frisch, M. J.; Trucks, G. W.; Schlegel, H. B.; Scuseria, G. E.; Robb, M. A.; Cheeseman, J. R.; Scalmani, G.; Barone, V.; Mennucci, B.; Petersson, G. A.; Nakatsuji, H.; Caricato, M.; Li, X.; Hratchian, H.

P.; Izmaylov, A. F.; Bloino, J.; Zheng, G.; Sonnenberg, J. L.; Hada, M.; Ehara, M.; Toyota, K.; Fukuda, R.; Hasegawa, J.; Ishida, M.; Nakajima, T.; Honda, Y.; Kitao, O.; Nakai, H.; Vreven, T.; Montgomery, J. A., Jr.; Peralta, J. E.; Ogliaro, F.; Bearpark, M.; Heyd, J. J.; Brothers, E.; Kudin, K. N.; Staroverov, V. N.; Kobayashi, R.; Normand, J.; Raghavachari, K.; Rendell, A.; Burant, J. C.; Iyengar, S. S.; Tomasi, J.; Cossi, M.; Rega, N.; Millam, J. M.; Klene, M.; Knox, J. E.; Cross, J. B.; Bakken, V.; Adamo, C.; Jaramillo, J.; Gomperts, R.; Stratmann, R. E.; Yazyev, O.; Austin, A. J.; Cammi, R.; Pomelli, C.; Ochterski, J. W.; Martin, R. L.; Morokuma, K.; Zakrzewski, V. G.; Voth, G. A.; Salvador, P.; Dannenberg, J. J.; Dapprich, S.; Daniels, A. D.; Farkas, O.; Foresman, J. B.; Ortiz, J. V.; Cioslowski, J.; Fox, D. J. *Gaussian 09*, revision D.01; Gaussian, Inc.: Wallingford, CT, 2009.

(42) Shuai, Z.; Peng, Q.; Niu, Y.; Geng, H. *MOMAP*, Revision 0.3.001; Beijing, China, 2016 (*MOMAP*: a free and open-source molecular materials property prediction package; available online <http://www.shuaigroup.net>).

(43) Valiev, M.; Bylaska, E. J.; Govind, N.; Kowalski, K.; Straatsma, T. P.; Van Dam, H. J. J.; Wang, D.; Nieplocha, J.; Apra, E.; Windus, T. L.; de Jong, W. A. *NWChem*: A comprehensive and scalable open-source solution for large scale molecular simulations. *Comput. Phys. Commun.* **2010**, *181*, 1477–1489.

(44) Gierschner, J.; Mack, H. G.; Egelhaaf, H. J.; Schweizer, S.; Doser, B.; Oelkrug, D. Optical spectra of oligothiophenes: vibronic states, torsional motions, and solvent shifts. *Synth. Met.* **2003**, *138*, 311–315.

(45) Sun, Y.; Li, Y.; Li, Y.; Ma, F. Electronic structure and optical physical properties of oligothiophenes. *Comput. Mater. Sci.* **2007**, *39*, 673.

(46) Tretiak, S.; Saxena, A.; Martin, R. L.; Bishop, A. R. Conformational dynamics of photoexcited conjugated molecules. *Phys. Rev. Lett.* **2002**, *89*, 097402.

(47) Telesca, R.; Bolink, H.; Yunoki, S.; Hadziioannou, G.; Van Duijnen, P. T.; Snijders, J. G.; Jonkman, H. T.; Sawatzky, G. A. Density-functional study of the evolution of the electronic structure of oligomers of thiophene: Towards a model Hamiltonian. *Phys. Rev. B: Condens. Matter Mater. Phys.* **2001**, *63*, 155112.

(48) Lin, S. H.; Chang, C. H.; Liang, K. K.; Chang, R.; Shiu, Y. J.; Zhang, J. M.; Yang, T. S.; Hayashi, M.; Hsu, F. C. Ultrafast dynamics and spectroscopy of bacterial photosynthetic reaction centers. *Adv. Chem. Phys.* **2002**, *121*, 1–88.

(49) Spano, F. C.; Silvestri, L. Multiple mode exciton-vibrational coupling in H-aggregates: Synergistic enhancement of the quantum yield. *J. Chem. Phys.* **2010**, *132*, 094704.